NASA Technical Memorandum 83732

Turbulence and Surface Heat Transfer Near the Stagnation Point of a Circular Cylinder in Turbulent Flow

Chi R. Wang
Lewis Research Center
Cleveland, Ohio

Prepared for the
Winter Annual Meeting of the
American Society of Mechanical Engineers
New Orleans, Louisiana, December 9–14, 1984

NASA

TURBULENCE AND SURFACE HEAT TRANSFER NEAR THE STAGNATION POINT OF A CIRCULAR CYLINDER IN TURBULENT FLOW

Chi R. Wang
National Aeronautics and Space Administration
Lewis Research Center
Cleveland, Ohio 44135

E-2210

ABSTRACT

A turbulent boundary layer flow analysis of the momentum and thermal flow fields near the forward stagnation point due to a circular cylinder in turbulent crossflow is presented. Turbulence modeling length scale, anisotropic turbulence initial profiles and boundary conditions were identified as functions of the crossflow turbulence intensity and the boundary layer flow far field velocity. These parameters were used in a numerical computational procedure to calculate the mean velocity, mean temperature, and turbulence double correlation profiles within the flow field. The effects of the crossflow turbulence on the stagnation region momentum and thermal flow fields were investigated. This analysis predicted the existing measurements of the stagnation region mean velocity and surface heat transfer rate with crossflow Reynolds number and turbulence intensity less than 250 000 and 0.05, respectively.

NOMENCLATURE

A_i	coefficients of Eq. (22), i = 1 to 7
a_i	turbulence amplification factor, i = 1, 2, and 3
B_i	coefficients of Eq. (23), i = 1 to 4
c	correlation factor for the Reynolds stresses
D	cylinder diameter
E	sum of the dimensionless Reynolds normal stresses
E_i	dimensionless Reynolds normal stress, i = 1, 2, and 3
F	dimensionless mean flow streamwise velocity
f_i	parametrical function of φ, i = 1, 2, and 3
G	flow variable
H	dimensionless mean temperature
ℓ	turbulence modeling length scale
Nu	Nusselt number
Pr	Prandtl number
Re_d	Reynolds number, $V'_\infty D/\nu_\infty$
S	dimensionless Reynolds shear stress, $-\overline{uv}/U_e^2$
T	mean temperature
Tu	crossflow turbulence intensity, $\sqrt{\overline{v_\infty^2}}/V'_\infty$
t	temperature fluctuation
U	mean flow velocity component along the X_1 direction
u	velocity fluctuation along the X_1 direction
V	transformed velocity of V'
V'	mean flow velocity component along the X_2 direction
v	velocity fluctuation along the X_2 direction
w	velocity fluctuation along the X_3 direction
X_i	coordinates in the physical plane, i = 1, 2 and 3
δ	stagnation point laminar boundary layer thickness
η	transformed coordinate along X_2
θ	dimensionless variable, $-\overline{vt}/U_e T_e$
ν	kinematic viscosity
ξ	transformed coordinate along X_1
φ	angle from the stagnation point
φ_0	the initial station
$\overline{\quad}$	time mean average

Subscripts

e	far field boundary condition
oe	far field boundary condition at the initial station
m	M grid point in the η direction

ρ pivot point or previous ξ station

w surface condition

∞ cross flow condition

INTRODUCTION

The momentum and thermal flow fields near the forward stagnation point of a circular cylinder in turbulent crossflow have been the focus of considerable study, (1 to 12). One objective has been to understand the enchancement of the surface heat transfer due to crossflow turbulence near the leading edge of a fluid system component. Existing experiments, (3 and 4), have shown that the local Nusselt number increased by 75 percent as compared with laminar flow conditions when the turbulence intensity was 3 to 5 percent. In the initial turbine design stage, the blade leading edge is often modeled as a circular cylinder in a turbulent crossflow. With the current high operational gas temperature, the turbulence in the gas stream significantly increases the leading edge heat transfer. Thus, prediction of the stagnation region surface heat transfer becomes vital to the turbine blade cooling design. To estimate this surface heat transfer rate, correlations derived from experimental data may be used. The alternative is to rely on theoretical analysis and numerical computation to obtain the surface heat transfer rate.

Many two-dimensional unsteady laminar boundary layer flow analyses have examined the flow field in the vicinity of a stagnation point with the main stream velocity fluctuating about a steady mean. This type of analysis predicted little or no effects of free stream oscillation on the surface heat transfer rate for a flat plate or circular cylinder. The experiments on flat plates agreed in general with these theoretical results. However, the experiments, (1 to 8), indicated a large increase in the heat transfer rate near the forward stagnation point of a circular cylinder. Theoretical studies, (9 and 10), showed that vortex stretching caused a substantial increase in the surface heat transfer rate on cylinders. Therefore, the phenomena associated with a circular cylinder in a turbulent flow appear to be much different from a flat plate boundary layer flow. As the turbulent stream moves towards the stagnation point, amplification (or attenuation) of the Reynolds stresses occurs due to the flow deceleration. Turbulence amplification because of vortex stretching also occurs as the flow turns and moves away from the stagnation point. These phenomena influence the thin boundary layer and, therefore, the surface heat transfer rate.

Smith, (5), used two-dimensional boundary layer theory to analyze the flow at the stagnation point on a circular cylinder. The eddy viscosity was assumed to be proportional to the turbulence in the free stream. The proportionality constant was determined from the experimental data. Reynolds analogy, with a turbulent Prandtl number of unity, was also employed. This analysis indicated a greater effect of turbulence on heat transfer than on skin friction. Similar analytical approach was used by Gorla, (11), to investigate the effects of unsteady free stream and free stream turbulence on skin friction at a stagnation point. The free stream turbulence effect on skin friction was found to be less than that was reported in (5). These existing analyses did not study the anisotropic turbulence flow field. Hijikata, (12), performed a theoretical and experimental study of the stagnation point anisotropic turbulence. An equation for the anisotropic turbulence was added to the $k-\varepsilon$ turbulence model to analyze the measurements. Maximum Reynolds normal stress was found at a location far away from the surface and the normal stress decreased continuously in the direction normal to the surface. His analysis also showed that the turbulence length scale effect on the surface heat transfer rate was small compared with the effect of turbulence intensity. Donaldson, (13 and 14), has developed a turbulent boundary layer flow analysis, the method of invariant modeling, to study boundary layer flow transition and generation of atmospheric-clear air turbulence. Using a turbulence modeling technique to form a closed system of conservation equations for turbulent flow field, the analysis can be used to investigate dynamics among the anisotropic turbulence and mean flow streamwise property gradients. Since large mean flow streamwise velocity gradient and anisotropic turbulence exist within the turbulent stagnation point flow field, the Reynolds analogy or the $k-\varepsilon$ turbulence model is not sufficient to analyze the flow field. Therefore, based on the method of invariant modeling, the present paper proposes a turbulent boundary layer flow analysis and a computational scheme to study the anisotropic turbulence flow field and its effect on the stagnation region surface heat transfer on a cylinder in turbulent flow.

Reported herein are the theoretical analysis and numerical computational procedure used in this study. A summary of the conservation equations is presented. The turbulence modeling length scale is defined as a function of the turbulence. The initial profiles and far field boundary conditions are related to the crossflow turbulence and the inviscid flow velocity. The conservation equations are written in finite difference forms. A computational scheme is developed and performed to simulate the existing experiments. The computational results are then discussed and compared with the existing measurements.

THEORETICAL ANALYSIS OF THE FLOWFIELD

The flow field of interest in the present study is a small region within 20° of stagnation point. A schematic of this flow region, together with the physical and transformed coordinate systems, are shown in Fig. 1. It is assumed that the mean flow is steady, incompressible two-dimensional turbulent boundary layer flow. The mean flow field is described by two-dimensional boundary layer flow continuity, momentum, and enthalpy equations. The momentum and enthalpy equations contain the turbulence double correlations, $\overline{uv}$ and $\overline{vt}$. These double correlations are related to other turbulence correlations and the two-dimensional mean flow field through the turbulence dynamic equations. An analysis using the turbulence dynamic equations to keep track of the turbulence double correlations was developed in (13 and 14). This type of turbulence analysis was employed in the present study. Following the details in (13 and 14), conservation equations to describe the turbulent stagnation point flow field were derived. This set of conservation equations requires turbulence modeling techniques to form a closed system of equations for the turbulent flow field investigation. Conservation equations and turbulence closure assumptions are given in (15). The turbulence modeling length scale, coordinate transformation, turbulent flow initial profiles and boundary conditions are pertinent to the results of the present investigation. They are described in the following sections.

Turbulence Modeling Length Scale

For the turbulent flat plate boundary layer flow analysis, the turbulent mixing length is usually

assumed to vary linearly in a small distance normal to the surface and then to remain constant, approximately 0.1 of the boundary layer thickness, across the rest of the boundary layer. In the present study, turbulence modeling length scale, with similar profile in the X_2 direction as the mixing length in a flat plate boundary layer, was used to model the higher order correlation terms (tendency-towards-isotropy terms, turbulence diffusion terms, and turbulence dissipation terms) in the turbulence dynamic equations. It was also assumed that increasing the crossflow turbulence intensity would increase the length scale near the surface. Thus, the pivot point location, $X_{2,p}$, moves towards the surface as crossflow turbulence increases. In the outer region, the length scale, ℓ_e, is approximately 0.1 of the theoretical stagnation point laminar boundary layer thickness, δ. This length scale profile is shown in Fig. 2. The proportional factor between $X_{2,p}$ and the turbulence, Tu, was found by matching the present computational results with the existing measurements (1 to 8).

Coordinate Transformation

The coordinate transformation is to provide scale factors in the X_1 and X_2 directions so that, in the numerical computation, the X_1 step size can be increased and the number of steps in the X_2 direction can be reduced. Using the transformation, a constant step size in X_2 can be used and the rate of change of the dependent variables in the X_1 direction is also much reduced.

The following similarity coordinate transformations were used here:

$$\xi(x_1) = \int_0^{x_i} (U_e/\nu)dx_1 \quad \text{and} \quad \eta(X_1,X_2) = U_e X_2/\nu/(2\xi)^{0.5}$$

An external far field mean flow velocity of $U_e = 2V'_\infty \sin\varphi$ was assumed. The dependent variables were also nondimensionalized:

$$F = U/U_e,\ H = T/T_e,\ S = -\overline{uv}/U_e^2,\ \theta = -\overline{vt}/U_e T_e,$$

$$E_1 = \overline{u^2}/U_e^2,\ E_2 = \overline{v^2}/U_e^2,\ \text{and}\ E_3 = \overline{w^2}/U_e^2.$$

Therefore, $E = E_1 + E_2 + E_3$.

Through mathematical manipulations, the conservation equations, (15), can be written in the following forms in the transformed coordinate system:

Continuity equation:

$$2\xi\partial F/\partial\xi + \partial V/\partial\eta + F = 0 \qquad (1)$$

where,

$$V = \frac{2\xi\nu F}{U_e}\partial\eta/\partial X_1 + (2\xi)^{0.5}\frac{V'}{U_e}$$

Momentum equation:

$$2\xi F\partial F/\partial\xi + V\partial F/\partial\eta$$

$$= \frac{2\xi(1-F^2)}{U_e}\partial U_e/\partial\xi + \partial^2 F/\partial\eta^2 + (2\xi)^{0.5}\partial S/\partial\eta \qquad (2)$$

Energy equation:

$$2\xi F\partial H/\partial\xi + V\partial H/\partial\eta$$

$$= -2\xi\frac{FH}{T_e}\partial T_e/\partial\xi + \frac{1}{Pr}\partial^2 H/\partial\eta^2 + (2\xi)^{0.5}\partial\theta/\partial\eta \qquad (3)$$

Turbulence equations:

$$2\xi F\partial E_1/\partial\xi + V\partial E_1/\partial\eta$$

$$= -2\xi\frac{4E_1F}{U_e}\partial U_e/\partial\xi + \frac{U_e}{\nu}\partial\,(\ell E^{0.5}\partial E_1/\partial\eta)/\partial\eta$$

$$+ \partial^2 E_1/\partial\eta^2 + 2S(2\xi)^{0.5}\partial F/\partial\eta$$

$$+ 2\xi\frac{\nu E^{0.5}}{\ell U_e}\frac{(E-3E_1)}{3}$$

$$+ 2\xi E_1\left(-2\partial F/\partial\eta - \frac{2\nu}{U_e}\partial F/\partial\eta\cdot\partial\eta/\partial X_1 - \frac{2\nu^2}{U_e^2\ell^2}\right) \qquad (4)$$

$$2\xi F\partial E_2/\partial\xi + V\partial E_2/\partial\eta$$

$$= 5\frac{U_e}{\nu}\partial\,(\ell E^{0.5}\partial E_2/\partial\eta)/\partial\eta + \partial^2 E_2/\partial\eta^2$$

$$+ 2\xi\frac{\nu E^{0.5}}{U_e\ell}\frac{(E-3E_2)}{3}$$

$$+ 2\xi E_2\left(2\partial F/\partial\xi + \frac{2\nu}{U_e}\partial F/\partial\eta\cdot\partial\eta/\partial X_1 - \frac{2\nu^2}{U_e^2\ell^2}\right) \qquad (5)$$

$$2\xi F\partial E_3/\partial\xi + V\partial E_3/\partial\eta$$

$$= -2\xi\frac{2E_3F}{U_e}\partial U_e/\partial\xi + \frac{U_e}{\nu}\partial\,(\ell E^{0.5}\partial E_3/\partial\eta)/\partial\eta$$

$$+ \partial^2 E_3/\partial\eta^2 + 2\xi\frac{\nu E^{0.5}}{\ell U_e}\frac{(E-3E_3)}{3}$$

$$- 2\xi E_3\frac{2\nu^2}{U_e^2\ell^2} \qquad (6)$$

$$2\xi F\partial S/\partial\xi + V\partial S/\partial\eta$$

$$= -2\xi\frac{2FS}{U_e}\partial U_e/\partial\xi + 3\frac{U_e}{\nu}\partial\,(\ell E^{0.5}\partial S/\partial\eta)/\partial\eta$$

$$+ \partial^2 S/\partial\eta^2 + (2\xi)^{0.5}E_2\partial F/\partial\eta$$

$$+ 2\xi S\left(-\frac{\nu E^{0.5}}{U_e\ell} - \frac{2\nu^2}{U_e^2\ell^2}\right) \qquad (7)$$

and,

$$2\xi F\partial\theta/\partial\xi + V\partial\theta/\partial\eta$$

$$= -2\xi \frac{F\theta}{T_e}\partial T_e/\partial\xi + 3\frac{U_e}{\nu}\partial\,(\ell E^{0.5}\partial\theta/\partial\eta)/\partial\eta$$

$$+ \partial^2\theta/\partial\eta^2 + (2\xi)^{0.5} E_2 \partial H/\partial\eta$$

$$+ 2\xi\theta\left(\partial F/\partial\xi + \frac{\nu}{U_e}\partial\eta/\partial X_1 \cdot \partial F/\partial\eta - \frac{\nu E^{0.5}}{U_e\ell} - \frac{2\nu^2}{U_e^2\ell^2}\right) \quad (8)$$

Equations (4), (5), (6), and (7) show the relationships among the Reynolds normal stresses, shear stress, and the mean flow velocity. Equations (3) and (8) relate the turbulence effect on the temperature field and, thus, the surface heat transfer rate. With the assumptions of the length scale for the turbulence modeling, Eqs. (1) to (8) were solved numerically for the momentum and temperature fields. The initial flow profiles and boundary conditions are analyzed in the following sections.

Initial Profiles

Because the crossflow turbulence affects the flow field, the initial profiles can not be assumed. They were determined analytically from the governing Eqs. (1) to (8). Assumptions for the mean flow streamwise gradients were made and the conservation equations were reduced to a set of ordinary differential equations. These equations were solved for the property profiles at the initial location, $\varphi = \varphi_o$. The analysis, with assumptions, is described here:

1. At $\varphi = \varphi_o$ and $X_2 \approx \infty$, $(\eta = 8.)$, $\partial F/\partial\eta = 0$, $\partial H/\partial\eta = 0$, $\partial E_1/\partial\eta = 0$, $\partial E_2/\partial\eta = 0$, $\partial E_3/\partial\eta = 0$, $\partial S/\partial\eta = 0$, and $\partial\theta/\partial\eta = 0$ were assumed. In addition, $F = 1$, $H = 1$, and $\theta = 0$ were imposed as boundary conditions at $X_2 \approx \infty$.

2. To determine the Reynolds normal and shear stresses, $E_1(\varphi, X_2) = E_1(\varphi_o, X_2)\,[U_e(\varphi_o)/U_e(\varphi)]^2$, and $E_2(\varphi, X_2) = E_2(\varphi_o, X_2)\,[U_e(\varphi_o)/U_e(\varphi)]^2$ were assumed in the vicinity of the stagnation point. Therefore:

$$\partial E_1/\partial\xi = E_1(\xi_o, X_2)\left(\frac{-2}{Re_d^2\,\varphi_o^2}\right) \quad (9)$$

and

$$2E_2/\partial\xi = E_2(\xi_o, X_2)\,\frac{-2}{(Re_d^2\,\varphi_o^2)} \quad (10)$$

were found for small φ_o. Similarly,

$$\partial E_3/\partial\xi = E_3(\xi_o, X_2)\, f_1(\varphi_o) \quad (11)$$

$$\partial S/\partial\xi = S(\xi_o, X_2)\, f_2(\varphi_o) \quad (12)$$

and

$$\partial\theta/\partial\xi = \theta(\xi_o, X_2)\, f_3(\varphi_o) \quad (13)$$

were assumed.

3. The mean flow is symmetric about $\varphi = 0$ plane. The mean flow streamwise velocity and temperature gradients are zero at $\varphi = 0$ plane. These mean flow properties were also assumed at locations near the stagnation point, $\varphi \approx 0$. Therefore, $\partial F/\partial\xi = 0$ and $\partial H/\partial\xi = 0$ were imposed along the X_2 direction at φ_o station.

4. The boundary conditions, $F = 0$, $H = T_w/T_e$, $V = 0$, $E_1 = 0$, $E_2 = 0$, $E_3 = 0$, $S = 0$, and $\theta = 0$, were also imposed at the surface $(X_2 = 0)$.

5. To determine the values of $E_{1,oe}$, $E_{2,oe}$, $E_{3,oe}$, and S_{oe} at $X_2 \approx \infty$,

$$U_{oe} = 2V'_\infty \sin\varphi_o \quad (14)$$

and

$$\overline{v_{oe}^2} = \overline{V_\infty^2} \quad (15)$$

were assumed at $X_2 \approx \infty$.

Applying the assumptions, (Eqs. (9) to (13)), to the governing Eqs. (4) to (8), the following results were found at $\varphi = \varphi_o$ and $X_2 \approx \infty$ $(\eta = 8.)$:

$$E_{1,oe} = \frac{\dfrac{\nu E_{oe}^{1.5}}{3U_{oe}\ell_e}}{\dfrac{-2}{Re_d^2\varphi_o^2} + \dfrac{4}{U_{oe}}(dU_e/d\xi)_o + \dfrac{\nu E_{oe}^{0.5}}{U_{oe}\ell_e} + \dfrac{2\nu^2}{U_{oe}^2\ell_e^2}} \quad (16)$$

$$E_{2,oe} = \frac{\dfrac{\nu E_{oe}^{1.5}}{3U_{oe}\ell_e}}{\dfrac{-2}{Re_d^2\varphi_o^2} + \dfrac{\nu E_{oe}^{0.5}}{U_{oe}\ell_e} + \dfrac{2\nu^2}{U_{oe}^2\ell_e^2}} \quad (17)$$

$$f_1(\varphi_o) = -\frac{2}{U_{oe}}(dU_e/d\xi)_o + \frac{\nu E_{oe}^{1.5}}{U_{oe}E_{3,oe}}\,\frac{1}{3\ell_e} - \frac{\nu E_{oe}^{0.5}}{U_{oe}\ell_e} - \frac{2\nu^2}{U_{oe}^2\ell_e^2} \quad (18)$$

$$f_2(\varphi_o) = -\frac{2}{U_{oe}}(dU_e/d\xi)_o - \frac{\nu}{U_{oe}}\frac{E_{oe}^{0.5}}{\ell_e} - \frac{2\nu^2}{U_{oe}^2\ell_e^2} \quad (19)$$

and,

$$f_3(\varphi_o) = 0 \quad (20)$$

where $E_{oe} = E_{1,oe} + E_{2,oe} + E_{3,oe}$. Substituting Eqs. (14) and (15) into Eqs. (16) to (19), $E_{1,oe}$, $E_{2,oe}$, $E_{3,oe}$, $f_1(\varphi_o)$, and $f_2(\varphi_o)$ were determined. With the assumptions in 2, the above parameters were used to define the mean flow streamwise turbulence gradient terms except $\partial S/\partial\xi$.

To determine the $\partial S/\partial\xi$ at the initial location φ_o, the following relations among the Reynolds stresses, i.e.,

$$S_{oe} = c\,(E_{1,oe}\,E_{2,oe})^{1/2} \quad (21)$$

at $X_2 \approx \infty$ was assumed. This relation is similar to that has been proposed for the flat plate boundary layer turbulence, (16). For the present study, the factor, $c = 0.0001$, was used.

Following the above detail, a set of ordinary differential equations with specified boundary conditions were established at φ_0 location. These equations were solved numerically for the initial profiles at $\varphi_0 = 0.0375°$ to avoid the singularity at the stagnation point.

Boundary Conditions

Surface and far field boundary conditions are required to analyze the downstream flow field. Phenomenological boundary conditions for E_{1e}, E_{2e}, and E_{3e} were inferred from the results of existing heat transfer measurements.

The surface heat transfer rate beneath a stagnation point flow field with given Re_d and Tu is approximately constant in $\varphi \leq 20°$. This surface heat transfer rate can be computed from the initial profile analysis. The Reynolds normal stresses, $\overline{u^2}_e$ and $\overline{v^2}_e$ and the cylinder axial direction Reynolds normal stress, $\overline{w^2}_e$, were derived from this heat transfer phenomenon. Numerical computation was performed to obtain satisfactory distributions of these Reynolds normal stresses to enable the numerical analysis to predict the surface heat transfer within $\varphi \leq 20°$. The numerical method is described in the following Numerical Computation section. A rapid increase in the Reynolds normal stresses was necessary to obtain numerically the constant surface heat transfer rate near φ_0. The rapid increase in the Reynolds normal stresses was consistent with the turbulence amplification along an accelerated streamline.

Summary of the boundary conditions is given in the following:

1. The turbulence amplification/attenuation factors are defined as $a_1 = \overline{u^2}_e/\overline{u^2}_{oe}$, $a_2 = \overline{v^2}_e/\overline{v^2}_{oe}$, and $a_3 = \overline{w^2}_e/\overline{w^2}_{oe}$. These factors are assumed to be only functions of the mean flow streamwise velocity. A set of a_1, a_2 and a_3 is presented in Fig. 3 together with the numerical results of surface heat transfer for $Re_d = 1.85 \times 10^5$ and $T_u = 0.03$.
2. The far field mean flow streamwise velocity is described by $U_e = 2 V_\infty \sin \varphi$.

The far field Reynolds normal stresses are:

$$E_{1e} = \overline{u^2}_e/U_e^2 = a_1 E_{1,oe} (U_{oe}/U_e)^2$$

$$E_{2e} = \overline{v^2}_e/U_e^2 = a_2 E_{2,oe} (U_{oe}/U_e)^2$$

$$E_{3e} = \overline{w^2}_e/U_e^2 = a_3 E_{3,oe} (U_{oe}/U_e)^2$$

while $E_{1,oe}$, $E_{2,oe}$ and $E_{3,oe}$ were previously determined from the initial profile analysis.

3. The following conditions, $F_e = 1$, $H_e = 1$, $\theta = 0$, and $S = c\,(E_{1e} \cdot E_{2e})^{0.5}$ were also imposed at the far field boundary, $\eta = 8$.
4. The surface boundary conditions at $\eta = 0$, are $F = 0$, $V = 0$, $H = T_w/T_e$, $E_1 = 0$, $E_2 = 0$, $E_3 = 0$, $S = 0$, and $\theta = 0$.

With the initial profiles at φ_0 and the above boundary conditions, the downstream flow field properties were found by a downstream marching numerical computational procedure to solve the finite difference equations corresponding to the governing Eqs. (1) to (8).

NUMERICAL COMPUTATION

The governing equations were written in finite difference forms to compute numerically the dependent variable distributions along the η direction at each ξ (or φ) station. The following finite difference scheme and computational procedure were used.

Finite Difference Scheme

Every one of the governing Eqs. (1) to (8) can be expressed in a general form as:

$$A_1 \partial G/\partial \xi + A_2 \partial G/\partial \eta = A_3 G + A_4 \partial (A_5 \partial G/\partial \eta)/\partial \eta + A_6 \partial^2 G/\partial \eta^2 + A_7 \qquad (22)$$

where $A_i (i = 1 \text{ to } 7)$ may be constants, functions of the fluid properties and their gradients, or the transformation coordinates.

For the initial profile calculation, the assumptions and results described in the initial profile section were used to define $\partial G/\partial \xi$. The finite difference approximation, $\partial G/\partial \xi = (G - G_p)/\Delta \xi$, where G_p is the variable at the previous ξ station, was employed for downstream computation. The following finite difference expressions were also used to approximate the derivatives along the η direction.

$$(\partial G/\partial \eta)_m = (G_{m+1} - G_{m-1})/(2\Delta \eta)$$

$$(\partial^2 G/\partial \eta^2)_m = (G_{m+1} - 2G_m + G_{m-1})/(\Delta \eta)^2,$$

and

$$[\partial (A_5 \partial G/\partial \eta)/\partial \eta]_m = [A_{5,m+1/2} G_{m+1} - (A_{5,m+1/2} + A_{m-1/2}) G_m + A_{5,m-1/2} G_{m-1}]/(\Delta \eta)^2$$

with

$$A_{5,m+1/2} = (A_{5,m+1} + A_{5,m})/2$$

$$A_{5,m-1/2} = (A_{5,m} + A_{5,m-1})/2$$

Substituting the above expressions into Eq. (22), the following form of the finite difference equation:

$$B_1 G_{m+1} + B_2 G_m + B_3 G_{m-1} = B_4 \qquad (23)$$

was obtained. The coefficients B_i ($i = 1$ to 4) are functions of A_i at node points $m + 1$, m, and $m - 1$. With the prescribed boundary conditions, the variable G at each node point m was calculated from Eq. (23) by simple successive-substitution method.

Computational Procedure

A trial-and-error iteration procedure was used. A flow chart for this numerical process was given in Fig. 4. The present computational procedures contain two main routines at each ξ station. First, the turbulent velocity flow field was calculated. This velocity flow field was then used to compute the corresponding temperature distributions. Similar numerical computation procedures were repeated at the next downstream location.

At each ξ station, the coefficients A_i were determined first. The variable profiles at the previous ξ station was used in the first iteration and the

updated values at the current ξ station were then used to determine the coefficients for the next iteration. However, the laminar stagnation point boundary layer profiles were used to compute the A_i in the first iteration of the initial profile calculation.

For the cases calculated in this study, the computational domain was limited to $0.0375^\circ \leq \varphi \leq 20^\circ$ and $\eta \leq 8$. Constant grid dimension ($\Delta\eta = 0.05$) in η direction and variable stepsize along the ξ direction ($\Delta\xi$ corresponding to $\Delta\varphi = 0.0375^\circ$ for $\varphi \leq 0.2^\circ$ and $\Delta\varphi = 0.2^\circ$ for $\varphi \geq 0.2^\circ$) were used.

RESULTS AND DISCUSSION

The above numerical computational procedure was applied to calculate the turbulence and the mean flow properties within 20° of the forward stagnation point of a circular cylinder in turbulent crossflow. The crossflow mean temperature was 333 K. The cylinder diameter was 10.15 cm and its surface temperature was constant at 278 K. The Prandtl number was 0.7. The magnitudes of the mean crossflow velocity and its turbulence were prescribed to have approximately the same cross flow Reynolds number and turbulence intensity as they were reported in the existing experiments. Therefore, the present analytical results could be compared with the measurements. The present computational results were derived with the assumption of $\overline{v^2} = \overline{v_\infty^2}$. These numerical results are described and discussed here.

1. The mean flow streamwise velocity profiles at the initial station ($\varphi = 0.0375^\circ$) with $Re_d = 2.50\times10^5$ and $Tu \leq 0.05$ are shown in Fig. 5. These profiles were also compared with the theoretical laminar boundary layer solution, (16). Crossflow turbulence increased the near surface mean streamwise velocity and decreased the mean velocity at locations far away from the surface. Existing velocity profile measurements, at $\varphi = 0^\circ$ with $Tu = 0.05$, (17), were also shown in Fig. 5. General agreement could be found from the comparison.

Examples of the computational results of the Reynolds stress profiles at the initial station are shown in Fig. 6. The Reynolds normal stresses increase and then decrease along the radial direction towards the surface. Near the surface, high E_2 Reynolds normal stress was calculated. These profiles are different from the Reynolds stress distributions within a flat plate turbulent boundary layer, (16).

2. The Nusselt number at the initial location was computed from the mean temperature profile. The numerical results with different crossflow Reynolds number are compared with existing experimental results, (5), in Fig. 7. The correlation between the Nusselt number, Reynolds number, and turbulence intensity from several existing experiments and the present analysis were also plotted in Fig. 8. The present analysis satisfactorily predicts the stagnation point surface heat transfer rate over the ranges of $Re_d \leq 2.5\times10^5$ and $Tu \leq 0.05$. Although lower surface heat transfer rate, as compared with the results in (5), was calculated, the present analysis predicted the stagnation point heat transfer rate correlations, (5 to 8), especially at small and large values of $Tu(Re_d)^{1/2}$. The numerical computational results also show that the parameter, $Nu(Re_d)^{-0.5}$, approaches a maximum value ($= 1.6$) at large $Tu(Re_d)^{1/2}$. This result is consistent with the stagnation point heat transfer assumption used in turbine blade heat transfer design, (18).

3. The mean flow streamwise velocity profiles at downstream locations are shown in Fig. 9 for case with $Re_d = 1.85\times10^5$ and $Tu = 0.03$. Large variation in this mean velocity component occurred in $\varphi \leq 0.15^\circ$. Although turbulence amplification was imposed along the outer boundary of the flow field, rapid mean flow acceleration reduced the turbulence double correlations with a factor of $1/U_e^2$. This reduction in the outer edge boundary conditions decreases the Reynolds stresses within the flow field. Thus, the mean flow streamwise velocity distribution tended toward the laminar boundary layer profile as flow moves downstream.

Examples of the computational results of the Reynolds normal stress profiles at downstream locations are shown in Fig. 10. High Reynolds normal stresses, especially the E_1 component, appear near the surface. Profiles with large E_1 and small E_2 near the surface were calculated at downstream locations near $\varphi = 20^\circ$. These results are similar to the Reynolds normal stress profiles in flat plate turbulent boundary layer. They are significantly different from the initial profiles in Fig. 6.

The Reynolds shear stress distributions at three downstream locations are given in Fig. 11. Maximum shear stress occurs near the surface and the location shifts towards the surface as flow moves downstream. These results also show that shear stress profile restores to the flat plate turbulent boundary layer profile at locations about $\varphi = 20^\circ$.

4. Profiles of the dimensionless mean temperature, H, and the turbulence correlation, θ, with $Re_d = 1.85\times10^5$ and $Tu = 0.03$ are shown in Fig. 12. Mean temperature profile variation only occurs near the stagnation point. Comparison with the laminar boundary layer temperature profile is also made. Crossflow turbulence increases the near surface mean temperature and decreases the mean temperature in the far field of the boundary layer. The θ profiles show a large surface normal gradient at the initial location ($\varphi = 0.0375^\circ$). As it can be seen from Eq. (8), large E_2 near the stagnation point induces this turbulence gradient. This large turbulence gradient then increases the mean flow temperature near the surface and, therefore, the surface heat transfer rate. Small values in θ was computed at downstream locations. The effect of the θ variation on the mean temperature is mostly limited to a region away from the surface.

5. In the downstream flow calculation, the turbulence amplification/attenuation factors were derived from the numerical computation to obtain an approximately constant Nusselt number distribution within $\varphi \leq 20^\circ$ region. With these boundary conditions, a negative Reynolds stress gradient was computed along most parts of the outer boundary of the computational domain. This is possible due to the existence of the mean flow velocity gradients. This negative gradient was reduced to approximately zero gradient at $\varphi = 20^\circ$ locations where the Reynolds stress profiles are similar to those of the flat plate turbulent boundary layer. These computational results implied that the assumption of zero Reynolds stress gradients as far field boundary conditions is valid at locations ($\varphi \geq 20^\circ$) away from the stagnation point.

6. The above results are subjected to the assumptions and constraints in the multi-equation Reynolds stress modeling to account for the anisotropic turbulence. The length scale of the crossflow turbulence could induce different turbulence intensity near the stagnation point, (17), and its surface heat transfer rate, (8). The crossflow turbulence length scale effect was not considered in the present study.

CONCLUSION

Turbulence length scale, anisotropic turbulence initial and boundary conditions for a theoretical and

numerical boundary layer flow analysis of the stagnation region momentum and thermal flow fields have been defined as functions of the incoming crossflow turbulence and mean flow velocity. Methods to define the length scale, initial and boundary conditions and their applications to calculate the turbulence double correlations, mean velocity and temperature, and the surface heat transfer around the stagnation point of a circular cylinder in a turbulent crossflow were described. From the comparisons with the existing measurements, the present analysis was found capable of predicting accurately the local surface heat transfer rate with the crossflow Reynolds number less than 2.5×10^5 and turbulence intensity up to 5 percent.

REFERENCES

1. Zapp, G. M., MS Thesis, Oregon State University, 1950.

2. Schnautz, J. A., "Effect of Turbulence Intensity on Mass Transfer from Plates, Cylinders, and Spheres in Air Streams," Ph.D. Thesis, Oregon State College, 1958.

3. Seban, R. A., "The Influence of Free Stream Turbulence on the Local Heat Transfer from Cylinders," Journal of Heat Transfer, Vol. 82, Ser.C, No. 2, May 1960, pp. 101-107.

4. Kestin, J., Maeder, P.F., and Sogin, H.H., "The Influence of Turbulence on the Transfer of Heat to Cylinders near the Stagnation Point," Zeitschrift fuer Angew andte Mathematik und Physik, Vol. 12, 1961, pp. 115-132.

5. Smith, M. C., and Kuethe, A. M., "Effects of Turbulence on Laminar Skin Friction and Heat Transfer," Physics of Fluids, Vol. 9, No. 12, Dec. 1966, pp. 2337-2344

6. VanFossen, G. J.: "An Experiment of the Surface Heat Transfer of a Circular Cylinder in Turbulent Flow," will be published as NASA Report.

7. Lowery, G. W., and Vachon, R. I., "The Effect of Turbulence on Heat Transfer from Heated Cylinders," International Journal of Heat and Mass Transfer, Vol. 18, Nov. 1975, pp. 1229-1242.

8. Kestin, J., and Wood, R. T., "The Influence of Turbulence on Mass Transfer from Cylinders," Journal of Heat Transfer, Vol. 93, Nov. 1971, pp. 321-326.

9. Sutera, S. P., Maeder, P. F., and Kestin, J., "On the Stability of Heat Transfer in the Stagnation Point Boundary Layer to Free Stream Vorticity," Journal of Fluid Mechanics, Vol. 16, Pt. 4, Aug. 1963, pp. 497-520.

10. Sutera, S. P., "Vorticity Amplification in Stagnation Point Flow and Its Effect on Heat Transfer," Journal of Fluid Mechanics, Vol. 21, Mar. 1965, pp. 513-534.

11. Gorla, R. S. R.: "Combined Influence of Unsteady Free Stream Velocity and Free Stream Turbulence on Stagnation Point Heat Transfer," ASME paper 83-GTJ-17, Oct. 1983.

12. Hijikata, H., Yoshida, H., and Mori, Y., "Theoretical and Experimental Study of Turbulence Effects on Heat Transfer Around the Stagnation Point of a Cylinder," Heat Transfer for 1982, Proceedings of the Seventh International Conference, Deutsche Gesellschaft fuer Chemisches Apparatewesen, Vol. 3, 1982, pp. 165-170.

13. Donaldson, C. duP., "A Computer Study of an Analytical Model of Boundary Layer Transition," AIAA Journal, Vol. 7, No. 2, Feb. 1969, pp. 271-278.

14. Donaldson, C., Sullivan, R. D., and Rosenbaum, H., "A Theoretical Study of the Generation of Atmosphere-Clean Air Turbulence," AIAA Journal, Vol. 10, No. 2, Feb. 1972, pp. 162-170.

15. Wang, C. R., "Turbulence Effects on the Turbine Blade Pressure Surface Heat Transfer Rate," under preparation as a NASA technical publication.

16. Schlichting, H., Boundary Layer Theory, 4th ed., McGraw, New York, 1960.

17. Kestin, J., and Richardson, P. D., "The Effects of Free-Stream Turbulence and of Sound Upon Heat Transfer," ARL 69-0062, Wright-Patterson AFB, Dayton, OH, April 1969.

18. Glassman, A. J., "Turbine Design and Application," NASA SPL-290, vol. 3, 1975.

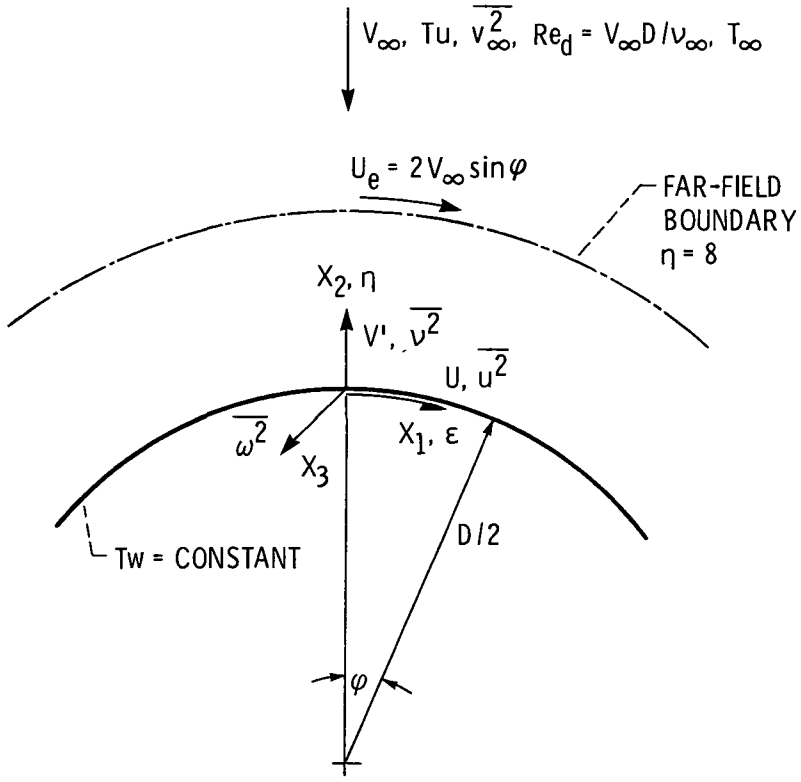

Figure 1. - A schematic of flow field of interest.

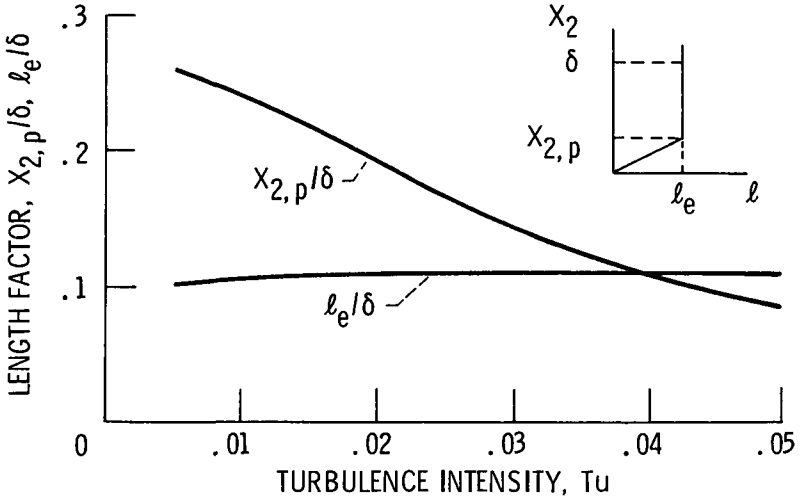

Figure 2. - Turbulence modeling length scale.

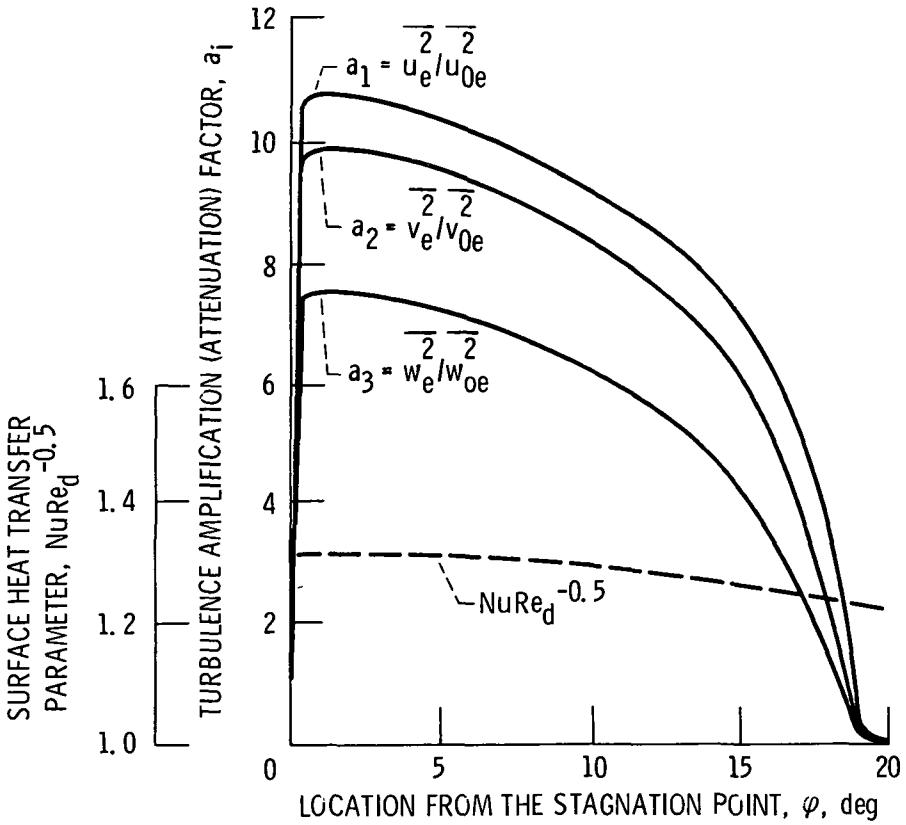

Figure 3. - Anisotropic turbulence boundary conditions and surface heat transfer correlation. Re_d, 1.85×10^5; Tu, 0.03.

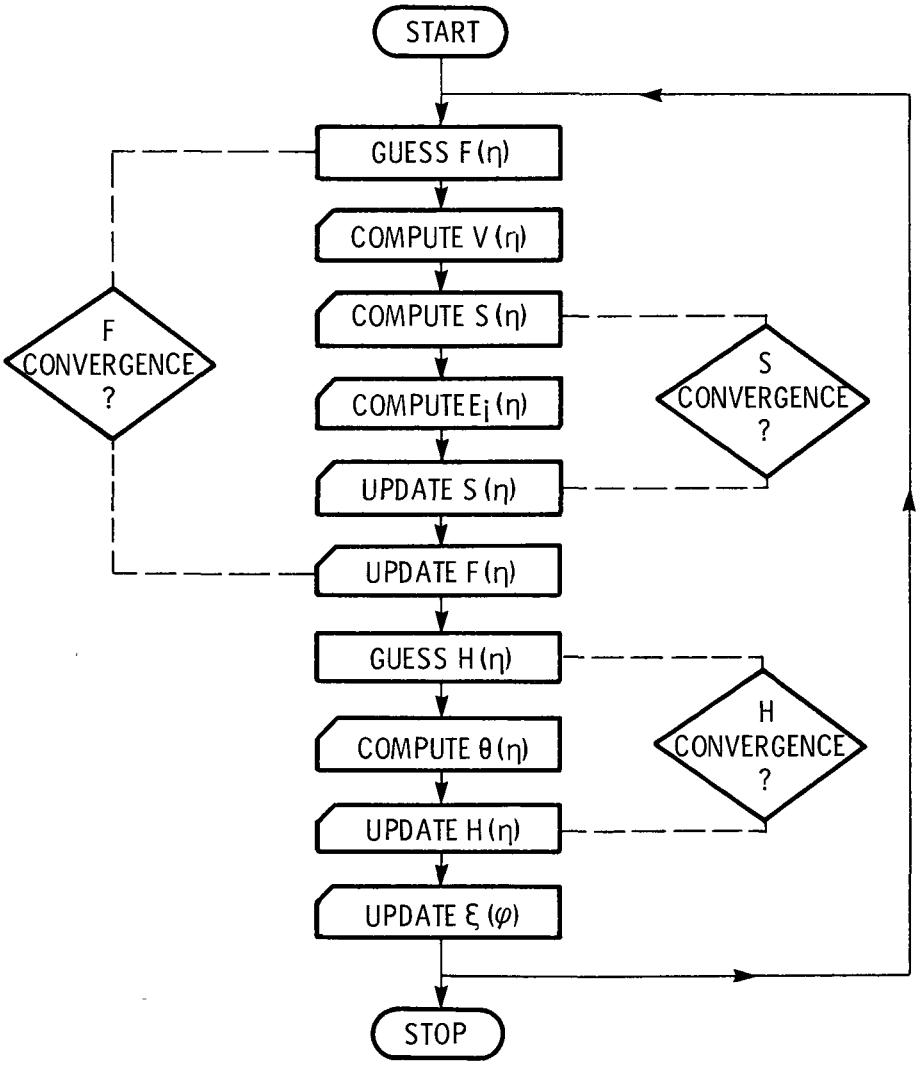

Figure 4. - Flow chart of the numerical computational procedures.

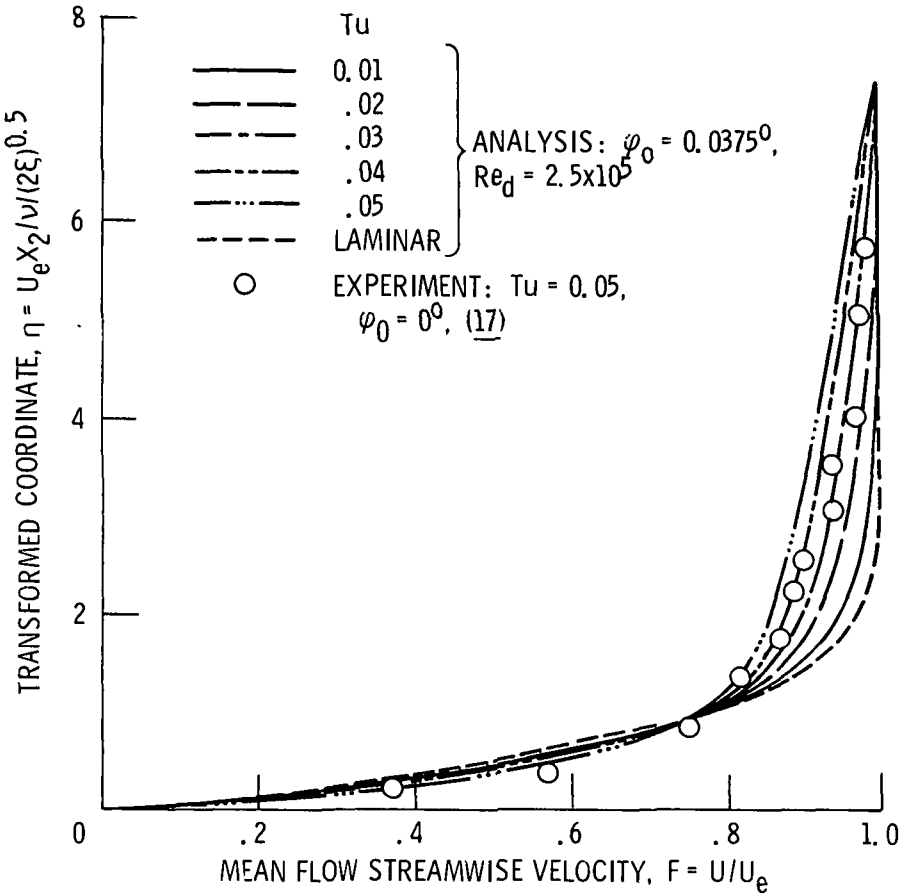

Figure 5. - Mean flow streamwise velocity profiles.

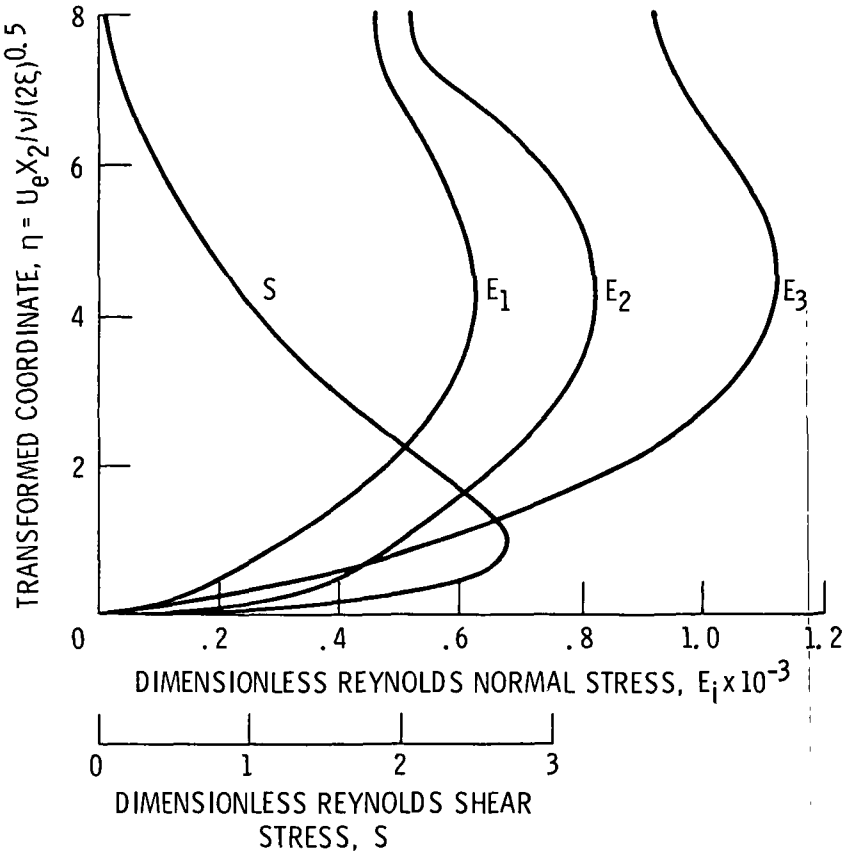

Figure 6. - Examples of Reynolds stress profiles at initial station, Re_d, 1.85×10^5; φ_0, 0.0375^0; Tu, 0.03.

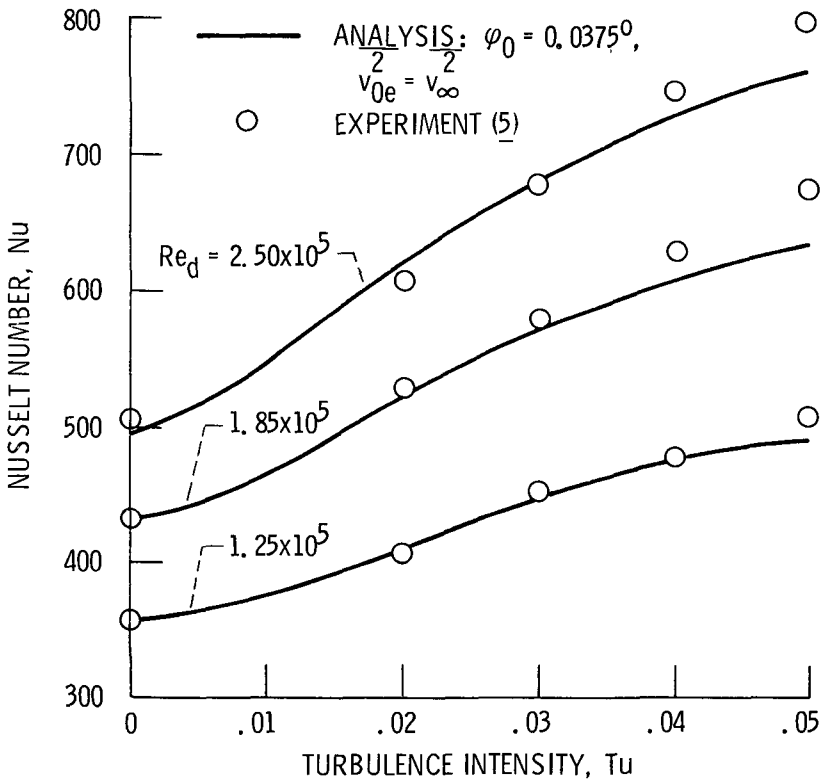

Figure 7. - Comparisons between analytical and experimental near stagnation point heat transfer.

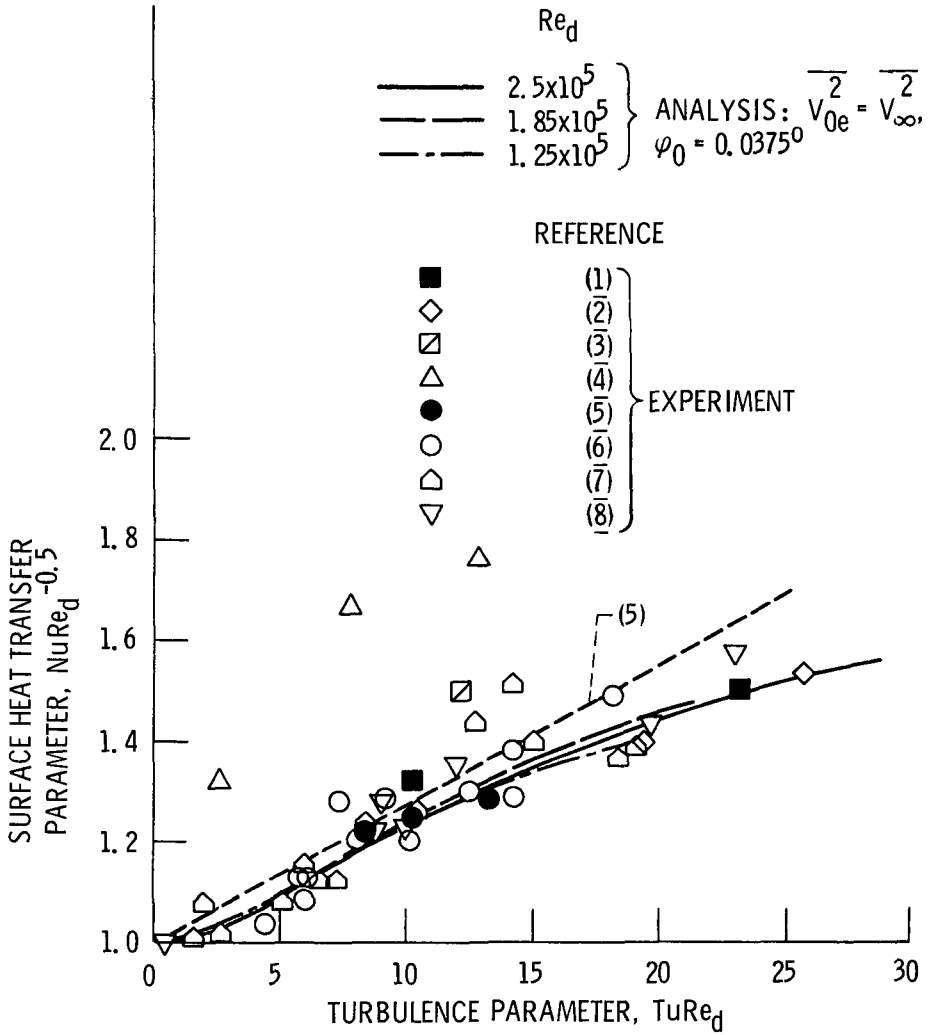

Figure 8. - Stagnation point heat transfer correlations from the analyses and experiments.

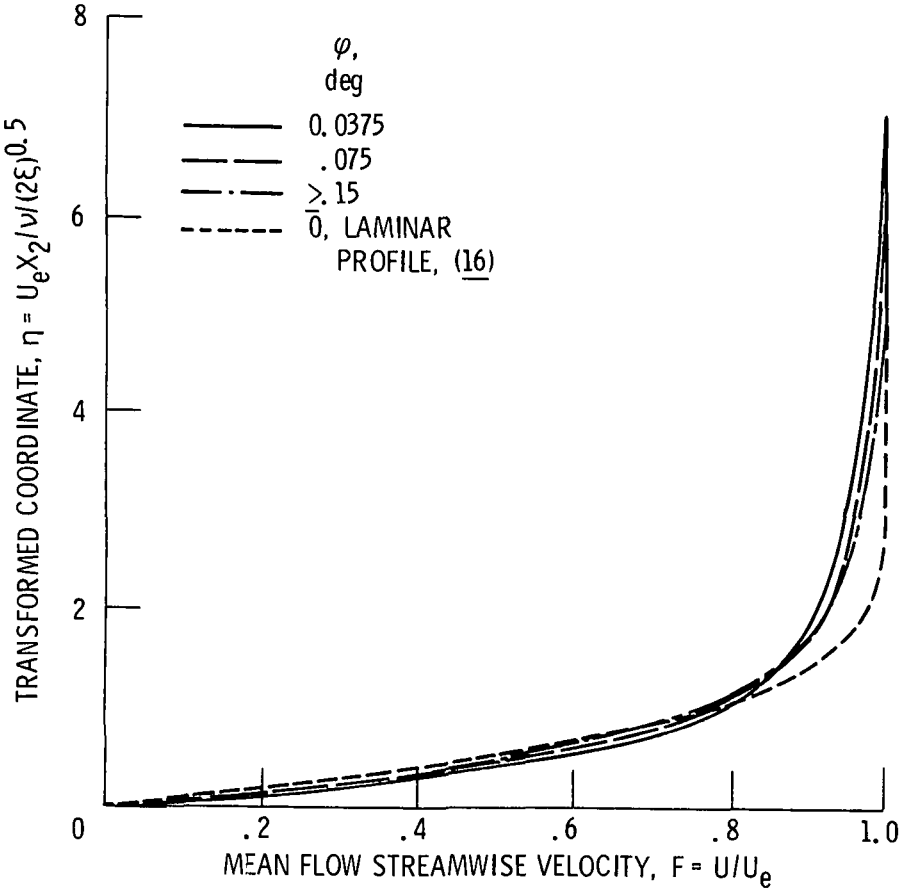

Figure 9. - Examples of mean flow streamwise velocity profiles at different locations. Re_d, 1.85×10^5; Tu, 0.03.

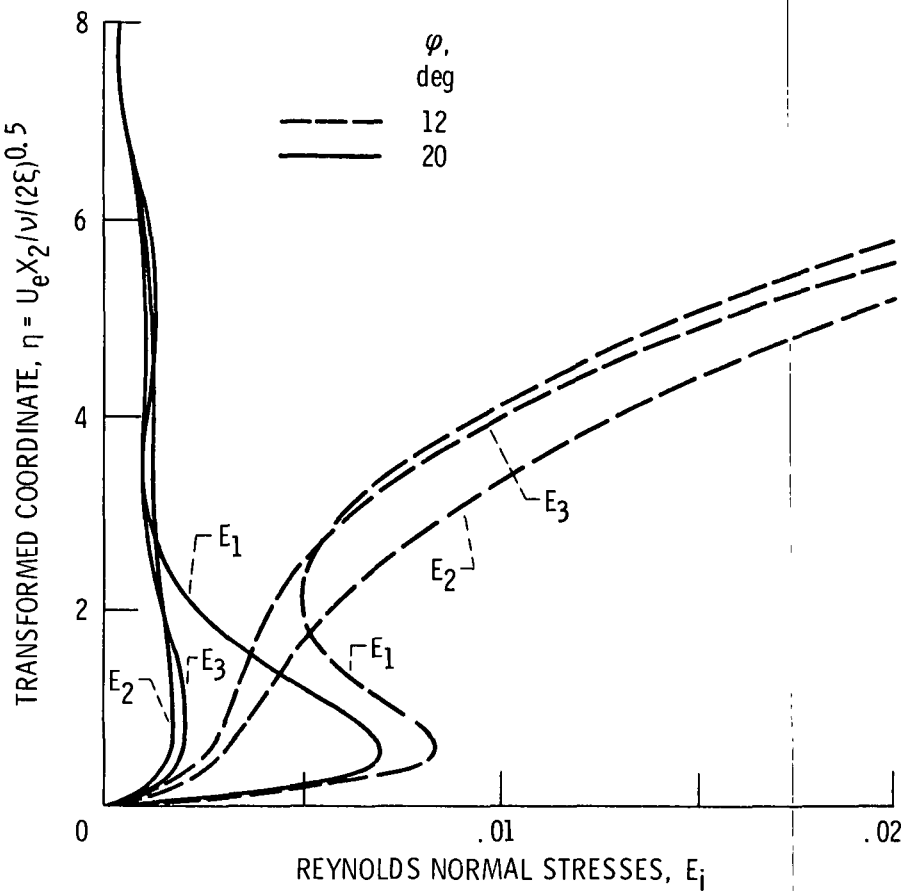

Figure 10. - Example of downstream Reynolds normal stress profiles. Re_d, 1.85×10^5; Tu, 0.03.

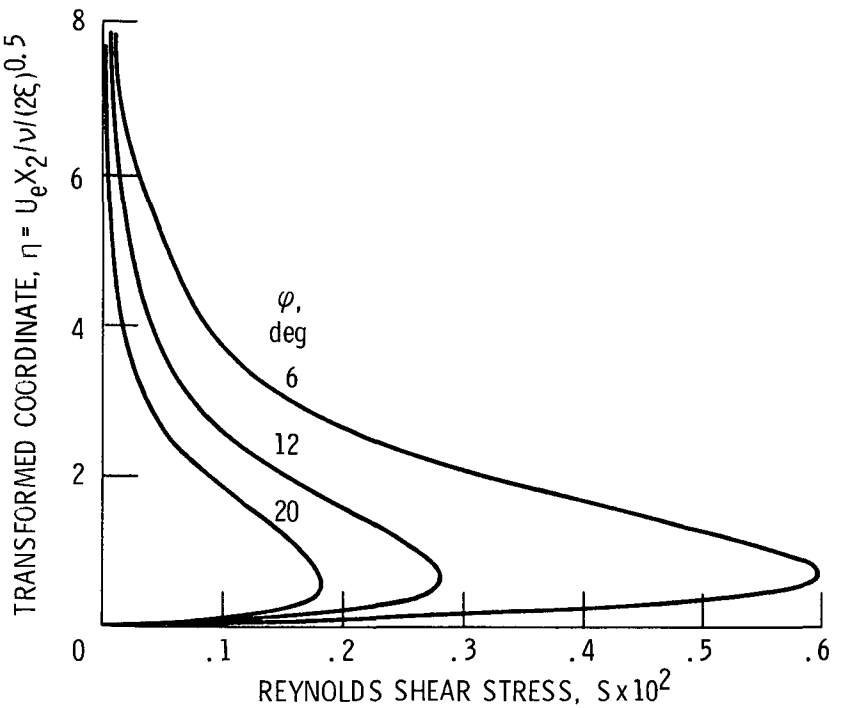

Figure 11. - Examples of downstream Reynolds shear stress profiles. Re_d, 1.85×10^5; Tu, 0.03.

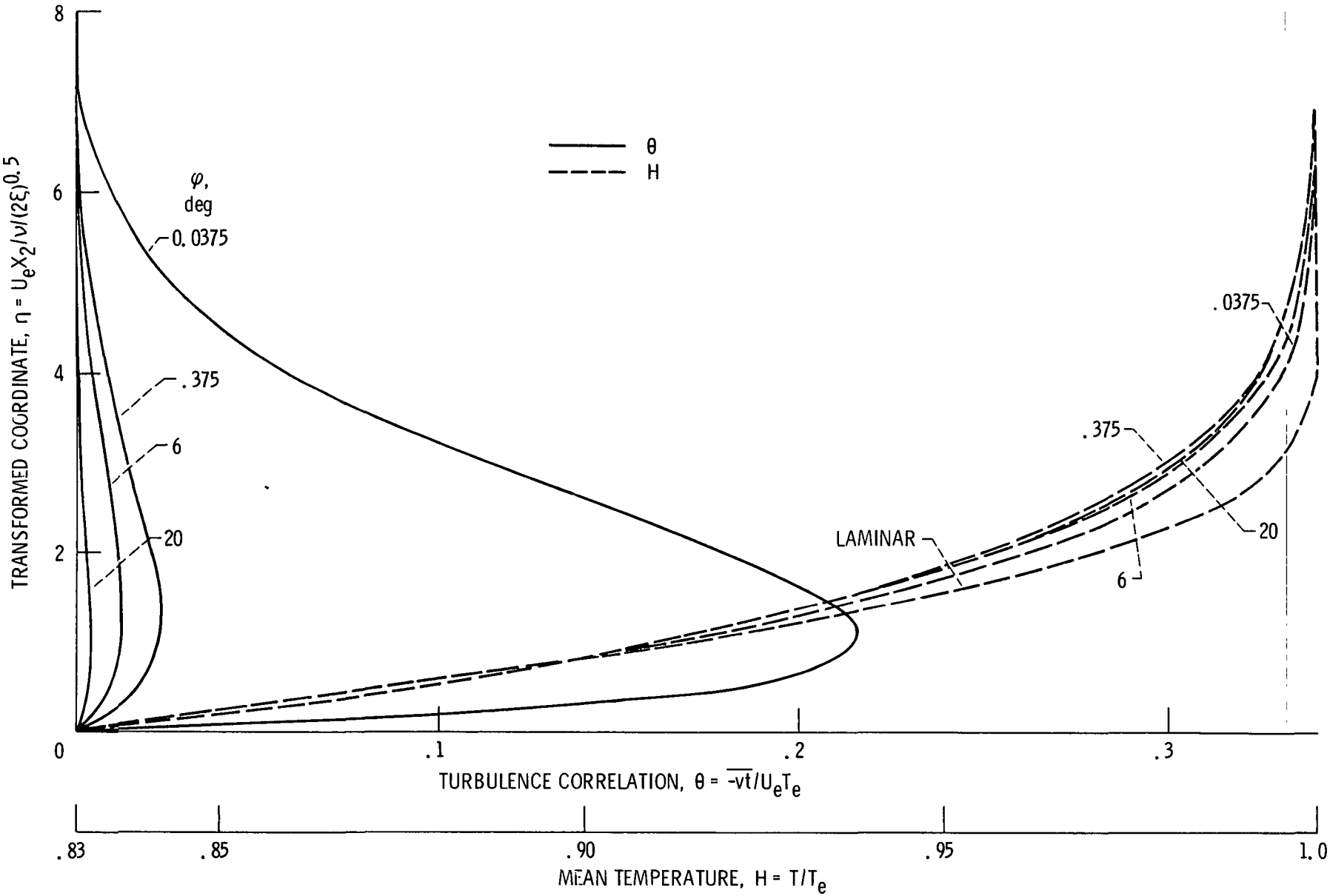

Figure 12. - Examples of the mean temperature and turbulence profiles. Re_d, 1.85×10^5; Tu, 0.03.

1. Report No.	2 Government Accession No	3 Recipient's Catalog No
NASA TM-83732		

4 Title and Subtitle	5 Report Date
Turbulence and Surface Heat Transfer Near the Stagnation Point of a Circular Cylinder in Turbulent Flow	6 Performing Organization Code 505-31-42

7. Author(s)	8 Performing Organization Report No
Chi R. Wang	E-2210
	10 Work Unit No

9 Performing Organization Name and Address	11. Contract or Grant No
National Aeronautics and Space Administration Lewis Research Center Cleveland, Ohio 44135	13. Type of Report and Period Covered Technical Memorandum

12 Sponsoring Agency Name and Address	14 Sponsoring Agency Code
National Aeronautics and Space Administration Washington, D.C. 20546	

15 Supplementary Notes

Prepared for the Winter Annual Meeting of the American Society of Mechanical Engineers, New Orleans, Louisiana, December 9-14, 1984.

16. Abstract

A turbulent boundary layer flow analysis of the momentum and thermal flow fields near the forward stagnation point due to a circular cylinder in turbulent crossflow is presented. Turbulence modeling length scale, anisotropic turbulence initial profiles and boundary conditions were identified as functions of the crossflow turbulence intensity and the boundary layer flow far field velocity. These parameters were used in a numerical computational procedure to calculate the mean velocity, mean temperature, and turbulence double correlation profiles within the flow field. The effects of the crossflow turbulence on the stagnation region momentum and thermal flow fields were investigated. This analysis predicted the existing measurements of the stagnation region mean velocity and surface heat transfer rate with crossflow Reynolds number and turbulence intensity less than 250 000 and 0.05, respectively.

17. Key Words (Suggested by Author(s))	18. Distribution Statement
Heat transfer Boundary layer Turbulence	Unclassified - unlimited STAR Category 34

19. Security Classif. (of this report)	20. Security Classif. (of this page)	21. No. of pages	22. Price*
Unclassified	Unclassified		

*For sale by the National Technical Information Service, Springfield, Virginia 22161

National Aeronautics and
Space Administration

Washington, D.C.
20546

Official Business
Penalty for Private Use, $300

SPECIAL FOURTH CLASS MAIL
BOOK

Postage and Fees Paid
National Aeronautics and
Space Administration
NASA-451

NASA

POSTMASTER: If Undeliverable (Section 158
Postal Manual) Do Not Return